Theoretical Study of CO and O_2 adsorption on $Ag_{32}Pt_6$ Nanoalloy

M.Sc. Thesis

by

TUSHAR GAJBHIYE

DEPARTMENT OF CHEMISTRY

INDIAN INSTITUTE OF TECHNOLOGY INDORE

MAY 2023

Theoretical Study of CO and O_2 adsorption on $Ag_{32}Pt_6$ Nanoalloy

A THESIS

Submitted in partial fulfillment of the
requirements for the award of the degree
of
Master of Science

by
TUSHAR GAJBHIYE

DEPARTMENT OF CHEMISTRY
INDIAN INSTITUTE OF TECHNOLOGY INDORE
MAY 2023

INDIAN INSTITUTE OF TECHNOLOGY INDORE

CANDIDATE'S DECLARATION

I hereby certify that the work presented in the thesis Theoretical Study of CO and O_2 adsorption on $Ag_{32}Pt_6$ Nanoalloy, which was submitted to the DEPARTMENT OF CHEMISTRY, Indian Institute of Technology Indore, is an authentic record of my own work completed during the time period from July 2022 to May 2023. This thesis is being submitted in partial fulfillment of the requirement for the award of the degree of MASTER OF SCIENCE, under the supervision of Dr. Satya S. Bulusu, Associate Professor, Department of Chemistry, IIT Indore.

TUSHAR GAJBHIYE

This is to certify that the above statement made by the candidate is correct to the best of my/our knowledge.

Dr. Satya S. Bulusu

TUSHAR GAJBHIYE has successfully given his M.Sc. Oral Examination held on **17 May 2023**

Signature of Supervisor of MSc thesis
Date: 20/05/2023

Convener, DPGC
Date: 25/05/2023

Signature of PSPC Member
Prof. Anjan Chakraborty
Date: 19/05/2023

Signature of PSPC Member
Prof. Sanjay Kumar Singh
Date: 23.05.2023

ACKNOWLEDGEMENTS

I would like to express my sincere gratitude to my supervisor Dr. Satya S. Bulusu for his invaluable guidance, encouragement, and support throughout the entire research project. His insightful feedback and constructive criticism were instrumental in shaping the direction of this study.

I am grateful to the staff and faculty of Chemistry Department for providing me with the resources, facilities, and opportunities to pursue my academic goals.

I would like to acknowledge the participants of this study, without whom this research would not have been possible. I appreciate their willingness to share their experiences and insights with me.

Lastly, I want to thank my family and friends for their unwavering support, encouragement, and patience during this journey. Their love and support have been my constant source of strength and motivation.

Thank you all for your invaluable contributions to my MSc thesis.

Tushar Gajbhiye

IIT Indore

Abstract

The theoretical study of CO and O_2 adsorption is an important area of research that can have a significant impact on the development of new materials and catalysts for various applications.

Optimizing catalyst design, energy storage, Predicting material properties and many more.

In this project we are using VASP for all the calculations related to computational studies of adsorption and using software's like VESTA and Chemcraft for visualizing the structure of cluster and then we tried to adsorb CO and O_2 on $Ag_{32}Pt_6$ nanoalloy and comparing our results with Ag_{38} nanocluster and verifying our results using methodology of Bader charge analysis.

Objective of our work is to identify the more feasibility of CO oxidation on $Ag_{32}Pt_6$ rather than Ag_{38}.

TABLE OF CONTENTS

LIST OF FIGURES

LIST OF TABLES

Chapter 1

Introduction

1.1 Nanoalloy

The variety of properties of metallic systems can be greatly increased by the use of mixtures of elements to produce intermetallic compounds and alloys. They have a wide range of uses in electronics, engineering, and catalysis [1] due to their great diversity of compositions, structures, and characteristics.[2] Bimetallic and multi-metallic alloy clusters, or "nanoalloys," have attracted a lot of attention lately due to the need to create materials with precisely defined, tunable features and architectures (on the nanoscale scale), as well as the adaptability offered by intermetallic materials. Research on nanoalloys that is based in theory and modelling is progressing along with experimental investigations (synthesis, characterization, and property measurement). [3]

The ability to tailor the composition, type, and degree of chemical ordering, as well as the size of the clusters, is one of the main factors contributing to the enormous surge in interest in nanoalloys. Due to finite size effects, nanoalloys frequently show structures and properties that are different from those of the pure elemental clusters and they may also show characteristics that are different from the corresponding bulk alloys. In many applications, particularly catalysis, the structures, compositions, and level of segregation or mixing of the surfaces of nanoalloys are also crucial factors. [4]

Materials made of two or more metallic elements at the nanoscale (usually between one and one hundred nanometers) are known as nanoalloys. These materials are small in size and have a large surface area, which provide them special qualities that are different from bulk alloys. [5] Chemical synthesis, vapour deposition, and electro deposition are just a few of the processes that

can be used to create nanoalloys. The use of nanoalloys in catalysis is among their most promising uses. Nanoalloys can catalyse chemical processes more effectively than their bulk equivalents due to their high surface area and distinctive electrical and geometric characteristics. Many researches have already been done on the catalytic uses of nanoalloys in fuel cells, hydrogen synthesis, and CO_2 reduction. Additionally, nanoalloys may find use in the fields of electronics, energy storage, and biomedicine.[6]

Nanoalloys have previously been used in a number of crucial technological fields, including optoelectronic, magnetic, and even medical applications. Examples include catalysis (such as electrochemical fuel cells and catalytic converters in automobiles).

1- Catalysis: Metals can be alloyed, or made into bimetallic solids, to change and fine-tune their properties, including their catalytic activity. The same is true for tiny metal atoms and clusters, and alloy nanocatalysis is presently gaining a lot of interest. According to *Christopher R. Schmid* ,[7] in the field of catalysis, the interaction between various neighbouring atoms can result in catalytic behaviour that is different from (and frequently better than) that of the monometallic clusters, i.e., "synergistic effects" are seen.

2- Optical Properties: DFT calculations can be used to produce more realistic simulations of plasmon spectra for smaller particles, which are now restricted to those with a mass of a few hundred atoms or less. The collapse of the plasmon model for smaller clusters, with optical spectra having many peaks, i.e., resembling those of ordinary molecules, is confirmed by DFT calculations on smaller clusters (e.g., from a few to some tens of atoms). For clusters of up to 10 atoms, time-dependent DFT calculations can also be done at a higher level of theory in order to calculate dynamic polarizabilities and derive optical spectra.[8]

3- Magnetic Properties: Granular substances created by embedding clusters in a solid host have attracted a lot of attention recently. Magnetic 3D metal

clusters (e.g., of Cr, Fe, Co, and Ni or mixtures of these metals) embedded in nonmagnetic metals or even insulators have been observed to exhibit the phenomenon of giant magneto-resistance (GMR), which can cause a change in resistance of up to 50% for Fe clusters embedded in Ag. [9] The research of bimetallic nanoalloys generated between magnetic 3d metals and nonmagnetic 4d (e.g., Rh, Pd, Ag) or 5d (e.g., Pt, Au) metals is the result of these GMR materials substantial promise for applications like magnetic sensors and magnetic recording. [10]

4- Biodiagnostics: The use of nanoparticles and other nanostructures in molecular diagnostics for biomedical applications has grown significantly in the last ten years. Examples include bio conjugation, cellular labelling, and assays for gases, metal ions, and DNA/protein markers for disease. Nanoparticles have the potential to increase robustness, sensitivity, and selectivity in this regard. Here is a brief introduction (in the context of nanoalloys); the interested reader is referred to *Rossi* and *Mirkin's* recent review of the area for more information. [11]

1.2 AgPt Nanoalloy

Pt-based nanoalloys in particular have drawn a lot of attention because of their use as heterogeneous catalysts in crucial reactions like the oxidation of CO to CO_2, hydrogenation of C=O, C=C, N=O bonds, and dehydrogenation of C-H and N-H bonds for the production of fuels and useful chemicals.[6] Additionally, it has been noted that the core-shell nanoalloys in comparison to their monometallic counterparts in the catalysis have a better utilisation of constituent atoms. Mixtures of Pt-Au, Pt-Ru, Pt-Rh, Pt-Cu, Pt-Co, Pt-Ni, and Pt-Ag are some of the Pt-based nanoalloys that have been extensively researched.[12]

In several theoretical and experimental investigations, combinations of the elements Au, Pd, and Pt have been described, and the catalytic activities have been examined.[13] By creating bimetallic Pd-Au dendrimer-

encapsulated catalysts, Crooks *et al.* discovered enhanced catalytic activity for the hydrogenation of allyl alcohols as compared to single metals in the presence of the alloy and core/shell Pd-Au nanoparticles.[14] Excellent catalytic performance for CO oxidation has been reported in experimental research on the catalytic activity of Au-Pt alloy nanoparticles.In comparison to Pt nanoparticles and a physical mixture of Pt and Au nanoparticles, the hydrogenation processes on Au-core Pt-shell bimetallic nanoparticles were more active.[15] These findings imply that the Au core causes platinum to be electron deficient. Pd-Ag bimetallic nanoparticles, on the other hand, were created at three different Pd:Ag ratios. A core-shell structure with Ag dominating the outer shell was produced by increasing the Ag:Pd ratio. Investigation of the catalytic activity revealed that the Ag presence enhances selectivity for alkyne hydrogenation. [16]

Additionally, because noble metals like Pt are typically very expensive. Alloying them with metals like Ag will enable the development of nanocatalysts that are both less expensive and extremely effective.

Ag-Pt nanoalloys reactivity is highly dependent on both their structure and composition, hence it is vital to identify their atomic-level geometrical and electronic structures in order to comprehend their catalytic capabilities. The nanoalloys have been the focus of numerous theoretical and experimental investigations during the past ten years. [17]

1.3 $Ag_{32}Pt_6$ cluster-

DFT-based research has been done on the structure, electronic characteristics, and interactions of small-sized Ag_nPt_n (n = 1-7) with CO molecules. It is discovered that Ag_4Pt_4 and Ag_6Pt_6, which have a closed geometric structure, are the two most stable clusters in the (n = 1-7) series.[18] According to this study, the Pt atoms interact with the CO molecule more strongly than the Ag atoms. As we move on to larger-sized nanoalloys, a

DFT-based investigation has been reported on the structure and stability of 54-atom $Ag_{45}Pt_9$ and 13-atom $Ag_{13-n}Pt_n$ using, respectively, an icosahedral cluster model and a (111) surface slab model. According to this study, structures with Pt atoms in the core location are formed by 13-atom Ag-Pt nanoalloys.[19] Additionally, it has been demonstrated that the clusters stability declines as Pt concentration rises. Mendes *et al.* recently examined the geometric and electrical characteristics of the 55-atom Pt-based transition metal(TM) nanoalloys Pt_nTM_{55-n} (n = 13, 42 and TM = Fe, Co, Ni, Cu, Ru, Rh, Pd, Ag, Os, Ir, Au), as well as the importance of charge transfer in the stability of these clusters. They discovered that the cluster's lowest energy isomer, $Pt_{13}Ag_{42}$, had an icosahedral structure with 13 Pt atoms constituting the cluster's core and 42 Ag atoms occupying its surface. [20]
Metropolis Monte Carlo (MC) simulations in conjunction with semi-empirical potential have been used to explore the configurations of larger Ag-Pt nanoparticles with 10-104 atoms. All Ag_mPt_n nanoalloys exhibit surface Ag segregation. According to previous research, when particle sizes or the overall Ag content in Ag-Pt nanoalloys increases, such segregation happens quickly. In a different study, structural investigation of Ag-Pt nanoalloys in the 10–100 nm size range was done utilising MC simulations with a unified embedded atom method potential model. [21] In this study, the chemical composition of Ag-Pt nanoalloys was altered to define multiple truncated octahedron (TO) forms. According to research, Pt-Cu nanoalloys have an onion-like TO structure, while Pt-Pd nanoalloys have mixed TO structures. Ag-Pt and Au-Pt nanoalloys have core-shell TO structures.
Given the discussion above, it is clear that there aren't many theoretical investigations into the systematic, objective structural prediction of Ag_mPt_n nanoalloys. Furthermore, understanding the adsorption characteristics of small, crucial molecules for the environment on Ag_mPt_n nanoalloys requires knowledge of their atomic-level structural details at finite temperatures. We have concentrated on the structural features of several medium-sized 38-

atom Ag_mPt_n nanoalloys. Previously, in our lab; the work had been done on it. [23]

The fact that 38 atoms corresponds to the so-called magic number cluster configuration is what drove my lab mentors to choose fcc-type 38-atom clusters with TO geometry (truncated octahedron). Because of the high degree of symmetry in the TO geometry, there are fewer "homotops" (i.e., isomers with the same size and composition but distinct spatial arrangements of chemical elements), which greatly simplifies the study of diffusion mechanisms. Additionally, the TO geometry of these nanoalloys competes with amorphous and icosahedral structures in this size range.

There were 8 possible isomers of $Ag_{38-n}Pt_n$ with lowest energy which was calculated using ANN and DFT based methods ($Ag_{37}Pt_1$, $Ag_{36}Pt_2$, $Ag_{35}Pt_3$, $Ag_{34}Pt_4$, $Ag_{33}Pt_5$, $Ag_{32}Pt_6$, $Ag_{31}Pt_7$ $Ag_{30}Pt_8$).[22]

They calculate the excess energy, E_{exc}, and the second order energy differential, Delta2E, for each of the distinct $Ag_{38-n}Pt_n$ nanoalloy compositions in order to assess their relative stability.

A stable composition in relation to its neighbour is often indicated by a positive value for $\Delta 2_E$. We show the extra energy in Fig. 1 as a function of the nanoalloys' composition. Given that $Ag_{32}Pt_6$ has the lowest value of Eexe in this figure, it is obvious that it is the most stable composition. In addition, we provide the Delta2E in Figure. 2 as a function of nanoalloy's composition. The $Ag_{32}Pt_6$ nanoalloy exhibits the greatest Delta2E value as well. A cluster that has a high positive value of Delta2E typically has great stability in comparison to its surrounding clusters. $Ag_{32}Pt_6$ is the most stable composition among the isomers, according to their analysis of excess energy and second-order energy difference. This is also compatible with the nanoalloy's flawless core-shell structure as shown in Figure 3.

The excess E_{Exc}, which is given in eq.1, has been used to investigate the relative stabilities of the Nanoalloys. [23]

$$E_{\text{exe}} = \frac{1}{38}\left[E_{\text{tot}}^{Ag_{38-n}Pt_n} - \frac{(38-n)}{38}E_{\text{tot}}^{\text{Ag}} - \frac{n}{38}E_{\text{tot}}^{\text{Pt}}\right] \quad \text{.....eq. 1}$$

$$\Delta_2 E_{Ag_{38-n}Pt_n} = \left[E_{\text{tot}}^{Ag_{38-n-1}Pt_{n+1}} + E_{\text{tot}}^{Ag_{38-n+1}Pt_{n-1}} - 2E_{\text{tot}}^{Ag_{38-n}Pt_n}\right] \quad \text{.....eq 2}$$

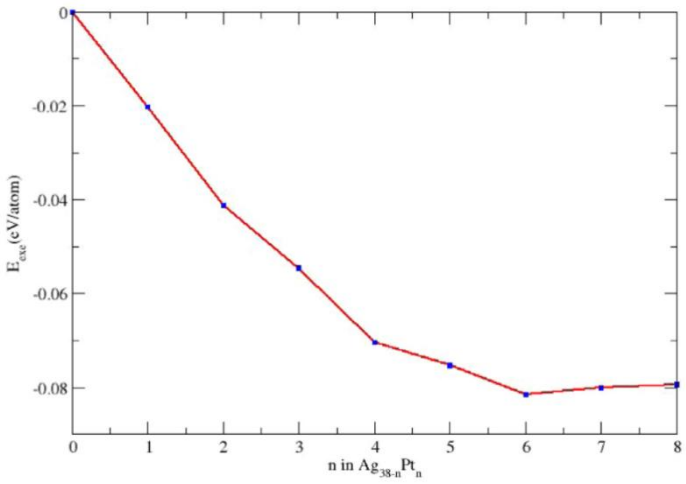

Figure 1. The excess energy plot with respect to the number of Pt atoms in 38-atoms Ag38-Ptn nanoalloy

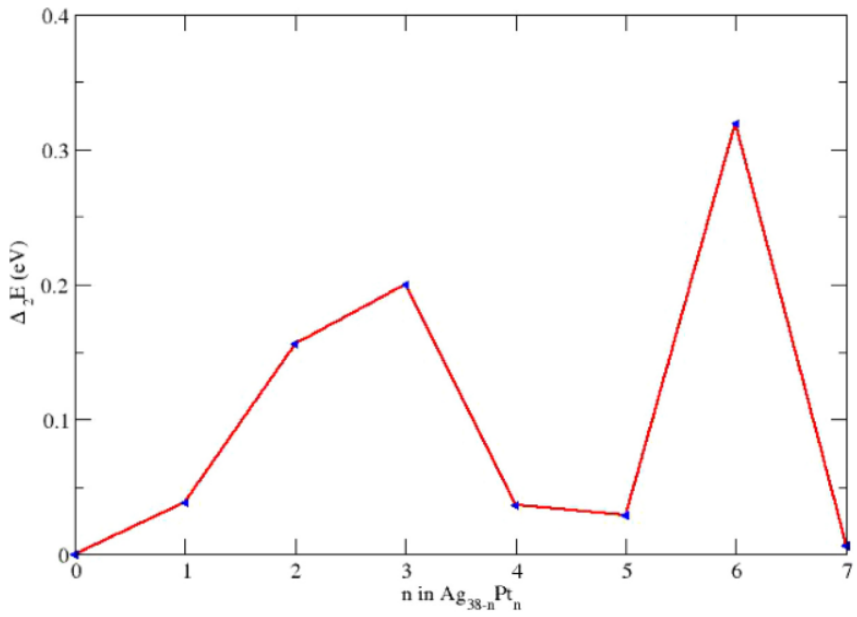

Figure 2. Plot shows the second order energy difference. The number of Pt atoms in 38-atoms energy differences with respect to the number of Pt atoms in 38 atoms $Ag_{38-n}Pt_n$ nanoalloy

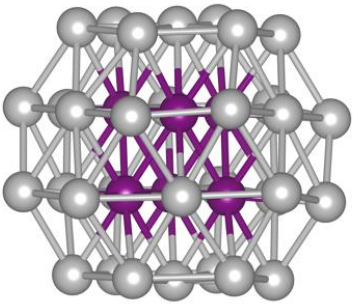

Figure 3.1. Structure of $Ag_{32}Pt_6$.

1.4 Ag_{38}

Ag_{38} cluster has unique square Ag_4 lattice. Ag_{38} has distorted octahedron or decahedron structure. It has 8 equilateral triangles and 6 square as its faces and 12 vertices. 13 surface silver atoms forming vertices of cubeoctahedron and 25 core silver atoms forming small octahedron inside the cubeoctahedron. Its geometry is affected by various factors as such the geometry of Ag_{38} nanocluster may not be suggested by single polyhedral structure.

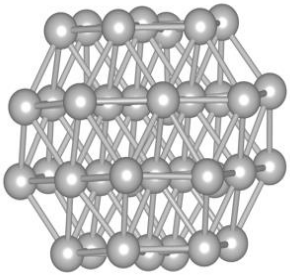

Figure 3.2. Structure of Ag_{38}

1.4 Adsorption-

The process of molecules or particles adhering to a surface is known as adsorption. The adsorbate (molecules or particles) in this process is drawn to the surface of the adsorbent (material), where it forms a thin film or layer. The adsorption process is brought about by the physical or chemical attractive forces between the adsorbent and the adsorbate .[24] Weak Van der Waals forces between the adsorbate and the adsorbent cause physical

adsorption, also known as Physisorption. There is no chemical reaction between the adsorbent and the adsorbate in this type of reversible adsorption. For gases and liquids adsorbed onto solid surfaces, physical adsorption is typical. Chemical bonds that form between the adsorbate and the adsorbent cause chemical adsorption, also known as chemisorption. Adsorbent and adsorbate undergo a chemical reaction during this form of adsorption, which is often irreversible. Atoms and molecules adhered to solid surfaces frequently undergo chemical adsorption. Many natural and technological systems depend on the fundamental process of adsorption. It is crucial for the separation of gases, water purification, the operation of catalytic materials, and the adsorption of molecules in biological systems, among other processes.

CO Adsorption:-

1. Catalysis: Catalytic processes may be impacted by CO adsorption on metal surfaces. In example, CO can be used as a probe molecule to examine the characteristics and surface structure of metals, assisting in the development of better catalysts.[24]

2. Gas sensing: As a toxic gas, CO must be detected for environmental and safety reasons. Adsorption of CO onto metal surfaces can alter their electrical conductivity or other characteristics, enabling the detection of the gas.

3. Surface science: One of the main areas of surface science, which aims to comprehend the interactions between molecules and solid surfaces, is the study of CO adsorption on metal surfaces. This information can be used to create new materials with particular qualities.

4. Corrosion: Metal corrosion behaviour may be impacted by CO adsorption on metal surfaces. For instance, CO can prevent metals from forming oxide layers, which can result in higher rates of corrosion. [25]

In conclusion, CO adsorption on metal surfaces is a significant area of study with prospective applications in catalysis, gas sensing, surface science, and corrosion prevention.

O_2 Adsorption:-

1. Catalysis: In many catalytic processes, such as the oxidation of alcohols, aldehydes, and hydrocarbons, O_2 adsorption on metal surfaces is an essential step. In these reactions, the organic molecules react with the O_2 molecules to produce the desired products after the O_2 molecules adsorb on the metal surface. The catalytic reaction can be facilitated by the adsorption of O_2 on metal surfaces, which can increase the metal's reactivity.[26]

2. Corrosion: Corrosion may also be influenced by the adsorption of oxygen on metal surfaces. Oxygen adsorption can result in the production of metal oxides on a metal surface, which can corrode the metal. However, in some circumstances, the development of a shielding oxide layer can stop further corrosion.

3. Surface chemistry: The chemistry of the metal's surface can also be impacted by O_2 adsorption on metal surfaces. For instance, it can change the metal surface's electrical characteristics, increasing or decreasing its reactivity towards other molecules. This may have effects on a number of applications, such as surface plasmon resonance and electrocatalysis. [27]

4. Sensors: It is also possible to create gas sensors by using the O_2 adsorption on metal surfaces. An optical or electrical change in the surface's conductivity or other characteristics caused by the adsorption of O_2 molecules on a metal surface can be detected by a sensor. This may be helpful for identifying O_2 in gas mixes or for keeping track of the amount of O_2 in the air.

O_2 adsorption on metal surfaces is a significant phenomenon with numerous real-world applications. We can create stronger corrosion inhibitors, better catalysts, and new sensors by comprehending the adsorption process.

Previously there is work done on adsorption for different Ag_mPt_n structures. [28]

It is discovered that Ag_9Pt_2 and Ag_9Pt_3 are incredibly powerful catalysts, with Ag_9Pt_2 setting a record by creating 1250 CO molecules per Pt atom per second at 300 °C. *Youp et.al*, [29] revealed the catalytic effectiveness of Ag-Pt nanoparticle supported by Al_2O_3 towards CO_2 oxidation in earlier work.

Using time-dependent density functional theory (TDDFT), the optical characteristics of bare Pt clusters and Ag_mPt_n nanoalloys have also been theoretically examined. The authors of this work primarily concentrated on clusters with icosahedral symmetry, ranging in size from 55 to 146 atoms. Their research demonstrated that a modest concentration of Pt atoms is sufficient to strongly quench the Ag Plasmon, causing an associated blue shift in the absorption peak. [30]

We are working on Adsorption of CO and O_2 on $Ag_{32}Pt_6$ nanoalloy using DFT.

Formula for calculation of adsorption energy.

$$E_{ads} = E_{Total} - E_{Bare} - E_{Atom\ attached} \qquad \text{Eq . 3}$$

Where E_{ads} is Adsorption energy, E_{total} is the total optimization energy of the cluster after adsorption, E_{Bare} is the optimization energy of the bare cluster before adsorption, and $E_{Atom\ attached}$ is the optimization energy of the atom (in our case CO and O_2) attached on bare cluster.

Chapter 2
Computational Details

2.1 VASP (Vienna Ab initio Simulation Package)

Density functional theory (DFT)-based first-principles electronic structure computations of materials are performed using the VASP (Vienna Ab initio Simulation Package) software. It is frequently used to research the electrical, optical, and structural aspects of materials in the fields of computational materials science and solid-state physics. The Materials Centre *Leoben Forschung GmbH* in Austria presently maintains and disseminates VASP, which was first created at the University of Vienna in Austria. It is a piece of commercial software that needs a licence to run.

The projector-augmented wave (PAW) method is used in the programme to explain the interaction between the electrons and the atomic nuclei and a plane-wave basis set to expand the electronic wave functions. Additionally, it has a number of sophisticated features like hybrid functionals, MBPT techniques, and non-equilibrium Green's function (NEGF) techniques. Metals, semiconductors, insulators, and organic materials are just a few of the many materials that VASP can model. It is utilised in a number of fields of research, including catalysis, surface science, condensed matter physics, and materials science. VASP is an effective tool for forecasting the properties of materials since it has undergone extensive benchmarking and validation against experimental data and other theoretical approaches. [31]

There are mainly 4 file in the input of VASP.

1- INCAR 2- KPOINT 3- POSCAR 4- POTCAR

1- INCAR

The VASP (Vienna Ab initio Simulation Package) software uses the INCAR file as a configuration file to manage the options and parameters for

electronic structure simulations that are carried out using density functional theory (DFT). Each keyword in the INCAR file specifies a different computation parameter or setting. With the help of these keywords, you can describe the specifics of an electronic structure calculation, including the calculation type (such as electronic minimization, geometry optimisation, or molecular dynamics), the functional type used for the exchange-correlation energy, the cutoff energy for the plane-wave basis set, the k-point sampling scheme, convergence criteria, and other calculation settings.
Some examples of keywords that can be specified in the INCAR file :
SYSTEM: Identifies the system being emulated by name.
PREC: Indicates the level of calculating precision (low, medium, or high).
ISTART: Defines the calculation's starting point (0 for a brand-new calculation, 1 for a restart).
ICHARG: Indicates the starting charge density (zero for a fresh computation, one for a recalculation).
ENCUT: Defines the plane-wave basis set's energy cut-off.
ALGO: Describes the electronic minimization algorithm (rapid, normal, or accurate).
ISMEAR: Describes the smearing technique used to determine the Fermi-Dirac distribution.
NSW: Defines the maximum number of ionic steps for a molecular dynamics simulation.
IBRION: Indicates the kind of ionic relaxation algorithm that is being utilised (for example, conjugate gradient, quasi-Newton, or damped molecular dynamics).

2- KPOINT

When calculating the electronic structure using density functional theory (DFT), the KPOINTS file in VASP specifies the Kpoint mesh that will be used to sample the Brillouin zone in reciprocal space. Understanding the electrical and optical characteristics of materials depends on the Brillouin

zone, a mathematical construct that depicts the periodicity of the crystal lattice.

The KPOINTS file in VASP normally has the following format:

1- The k-point mesh style, such as "Automatic" or "Line-mode," is specified in the first line.

2- The second line lists the number of KPOINT in the Brillouin zone in each direction.

3- The shift of the KPOINT mesh is specified in the third line and can be used to centre the k-point mesh on a particular location in the Brillouin zone.

4- The last four lines give the mesh's KPOINT' coordinates as well as any optional weightings.

3- POSCAR

The Vienna Ab initio Simulation Package (VASP) uses the POSCAR file as an input file to specify the crystal structure of the material under simulation. It includes details on the crystal structure's lattice characteristics and atomic locations.

The POSCAR file specifically includes the following data:

1- Comment line: A succinct explanation of the crystal structure.

2. Scaling factor: A scaling factor that establishes the size of the unit cell.

3. Lattice vectors: The lattice vectors that specify the crystal's unit cell.

4- Atomic species: A list of the chemical names for each element in the crystal.

5- Amount of atoms: The quantity of atoms in the crystal for each element.

6- Atomic positions: The Cartesian coordinates for each atom in the crystal.

Either fractional coordinates or Cartesian coordinates can be used to specify the atomic positions. The fractional coordinates along each lattice vector are used to represent the atomic positions. The atomic positions are specified as the precise coordinates in space in Cartesian coordinates. For VASP simulations, the POSCAR file is a crucial input file that needs to be carefully made in order to produce accurate results. It is frequently produced

utilising tools for modelling materials or software for visualising crystal structures. In my initial day, I made many mistakes in generating POSCAR file.

4- POTCAR

The pseudopotentials that are used to characterise the core electrons in a material are described in the POTCAR file of the Vienna Ab initio Simulation Package (VASP).

To treat the core electrons, which are closely bonded to the atomic nuclei and have little bearing on a material's electronic properties, pseudopotentials are a typical approximation used in electronic structure computations. Calculations can be performed more effectively by substituting effective potentials that are simpler to manage computationally for the core electrons using pseudopotentials.

The information on each atom's pseudopotential in the system under investigation can be found in the POTCAR file in VASP. The atomic symbol, the pseudopotential type (such as ultrasoft or projector-augmented wave), and the pseudopotential generation parameters are all included. The proper POTCAR file for each component of the system under study must be included when doing a VASP computation. This guarantees that the core electrons in each atom are described using the appropriate pseudopotentials, which is essential for generating reliable results for the electronic structure. The POSCAR file is made using the program which was given to me but everytime we are using it for different clusters we have to update the program like for $Ag_{32}Pt_6$ it will generate different POSCAR and for $Ag_{32}Pt_6CO$ different and for $Ag_{32}Pt_6O_2$ different file, so it had to be updated.

After running these files many output data are generated among which OUTCAR and CONTCAR are more important.

1- OUTCAR

The program's computations for the electronic structure are described in great detail in the OUTCAR file in VASP. It is one of the most significant output files produced by VASP and is jam-packed with knowledge on the electronic characteristics of the system under investigation.

The OUTCAR file contains details like :

1. Convergence data: Data on the convergence of the electronic self-consistent field (SCF) computation, including the maximum residual force, maximum residual stress, and the convergence threshold for energy and forces, are contained in the OUTCAR file.

2- Information on the electronic band structure, density of states (DOS), and projected density of states (PDOS) of the system under investigation are all included in the OUTCAR file. This provides details on the energy eigenvalues, orbital traits, and electronic state occupation numbers.

3. Information on ionic relaxation: If the computation included ionic relaxation, the OUTCAR file contains data on the forces acting on each atom, their final locations, and the total energy of the relaxed structure.

4- Additional data: The OUTCAR file may additionally include additional data, such as the basis set type, exchange-correlation functional type, and calculation's KPOINT sampling strategy.

It offers a plethora of knowledge regarding the electronic composition and characteristics of the system under investigation.

2- CONTCAR

The relaxed (i.e., optimised) structure's final atomic coordinates and lattice vectors are contained in the CONTCAR file in VASP following a geometry optimisation or a molecular dynamics simulation. It is a plain-text file that VASP creates in the POSCAR file format, a common format for describing the crystal structure of materials. The atomic coordinates and lattice vectors of the optimised structure are updated in the CONTCAR file, which contains the same data as the POSCAR file. The system is introduced in the

file's opening comment line, which is followed by a line that provides the lattice vectors' scaling factor. The lattice vectors in Cartesian coordinates are presented in the next three lines.

The file then lists the atomic species and how many of each species there are in the unit cell after the lattice vectors. The atomic coordinates in Cartesian coordinates are modified from the original coordinates supplied in the POSCAR file to reflect the optimised structure. This is followed by a block of lines. The final structure of the system following a relaxation or simulation is provided in the CONTCAR file, a crucial output file in VASP that can be utilised for additional analysis or as an input for subsequent calculations.

2.2 Chemcraft

Chemcraft is a computational chemistry graphical user interface (GUI) tool for visualising and evaluating electronic structure calculations. It is frequently used for activities including displaying molecular orbitals, visualising vibrational modes, examining transition states, and computing molecular characteristics in the field of theoretical and computational chemistry. *Grigoriy Zhurko*, a computational chemist based in Russia, created Chemcraft. Although it is a piece of commercial software, it provides a free trial version for use in academic settings. [32]

Programmes for calculating electronic structure, such as Gaussian, ORCA, GAMESS, NWChem, and many others, are supported by the software. In order to visualise the electronic structure of molecules and materials, it can read and analyse output files from these programmes and produce a variety of plots and diagrams. The user interface of Chemcraft is created to be simple to use and intuitive, and it includes a number of tools and capabilities that let users alter and examine electronic structure data. Molecular visualisation, energy profile graphs, molecular orbitals, electrostatic potential maps, and NBO analysis are just a few of the things it offers. Chemcraft is a useful tool for computational and theoretical chemistry

researchers since it makes it simple and quick to visualise and analyse electronic structure data.

2.3 VESTA

Crystal structures, electron densities, and other data pertaining to materials are visualised using the 3D visualisation programme VESTA in the fields of materials science and crystallography. The GNU General Public Licence allows for its free download and use. Takeshi Kasuga created it at the University of Tokyo in Japan. CIF, POSCAR, CHGCAR, and Cube files, among others, are among the file types that are frequently used in crystallography and materials research and are readable by VESTA. Users can edit the 3D visualisation of the structure using a range of tools and features after the data has been put into VESTA, including rotating, scaling, and translating the structure. To highlight particular parts of the structure, they can also alter the colours and visual representations of the atoms, bonds, and other properties. VESTA can analyse the data in many different ways, including visualising crystal structures, calculating bond lengths and angles, calculating coordination numbers, and creating symmetry-related structures. Additionally, it can produce top-notch graphics and images that are appropriate for publication and presentation. In materials science and crystallography, VESTA is a commonly used tool that is especially helpful for visualising complex structures and for getting insights into the characteristics and behaviours of materials at the atomic level. [33]

Uses of VESTA

1. Crystal structure visualisation: Crystallographic information files (CIFs), which are frequently used to store crystal structures, can be read and displayed by VESTA. Users can see crystal structures in a variety of ways, such as thermal ellipsoids, polyhedra, and ball-and-stick representations.

2- Crystal structure analysis: VESTA offers a variety of methods, including coordinate number analysis, bond valence sum calculations, and distance

and angle measurements. Additionally, it enables users to visualise crystal defects and disorder as well as generate symmetry-related crystal structures.
3. Molecular structure visualisation: VESTA can read and show molecular structure files, including Protein Data Bank (PDB) files, and it enables users to see molecules in a variety of ways, such as stick, ball-and-stick, and space-filling models.
4- Production of graphics suitable for publication: VESTA enables users to produce crystal and molecular structure graphics and images of the highest calibre for use in publications and presentations in the sciences. It allows for a wide variety of colour, label, and orientation customization choices and supports the export of graphics in a number of different formats, including vector drawings and high-resolution.

Chapter 3
Methodologies

3.1 Methodologies of VASP

We are trying to adsord CO and O_2 on $Ag_{32}Pt_6$ nanoalloy.

We are taking different sites of Ag to adsorb CO and O_2 as Pt is inside the core.

CO on $Ag_{32}Pt_6$ nanoalloy.

CO is adsorbed linerally.

O_2 is in bent form.

Other O_2 is in bridge form.

For $Ag_{32}Pt_6$ cluster we are taking 4 different sites of Ag and calculating their energies and then comparing those positions. And for maying bond between Ag and C and O we are using chemcraft and to calculate the energy we are using VASP and for visualising we are using Vesta.

Method of Geometry Optimization using VASP:

Step 1: Adsorption of molecule visualising in Chemcraft and obtaining Cartesian Coordinates

Step 2: Cartesian coordinates --> POSCAR file

Step 3: POSACAR, POTCAR, INCAR and KPOINTS files are in one folder

Step 4: Command: mpirun -np 16 /(folder of vasp) > 1 &

OUTCAR and CONCAR files are obtained

Optimized structure obtained from CONTCAR value and visualizing it with VIESTA software.

A. Adsorption of CO on $Ag_{32}Pt_6$ nanoalloy at 4 different sites.

Non-Optimized Structure

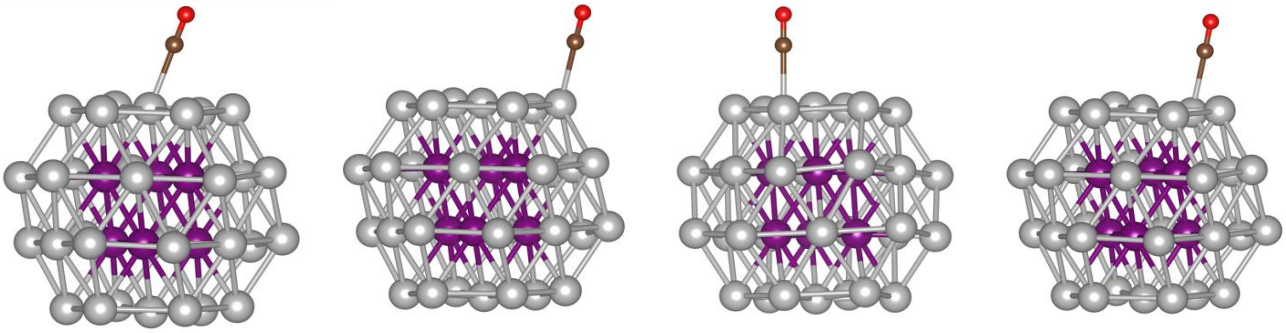

I A IB I C ID

Optimized Structure

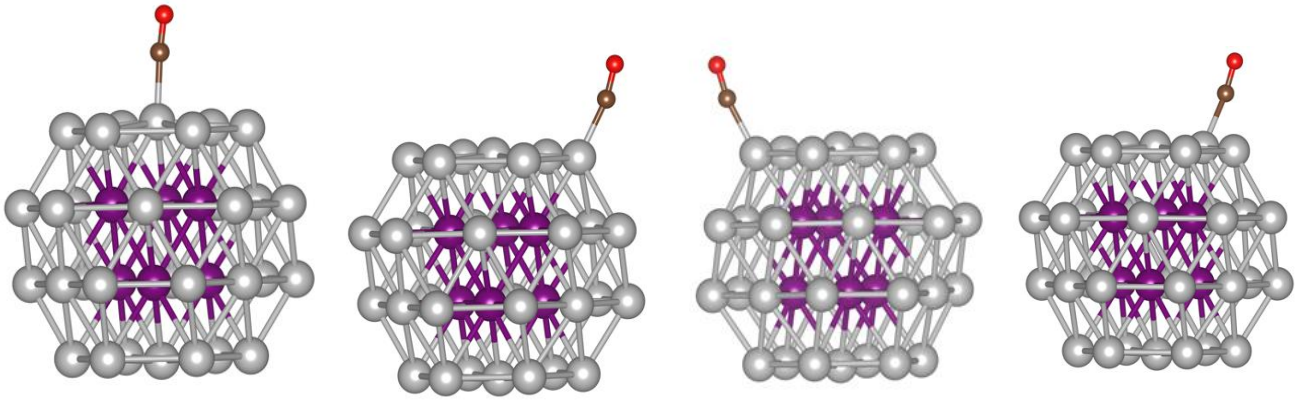

II A IIB IIC IID

Figure 4. IA,IB,IC,ID represents non optimised structures and IIA,IIB,IIC,IID represents optimised structures of $Ag_{32}Pt_6CO$.

B. Adsorption of O_2 on $Ag_{32}Pt_6$ nanoalloy at 4 different sites.

Non-Optimized Structure

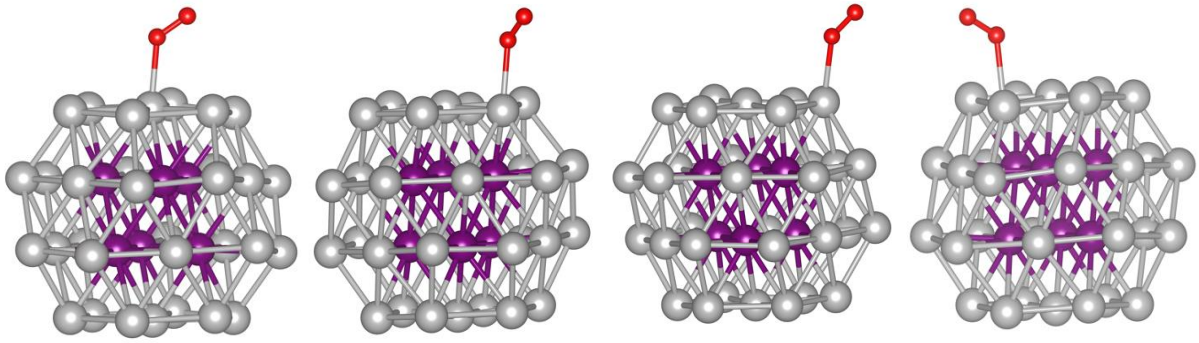

IA IB IC ID

Optimized Structure

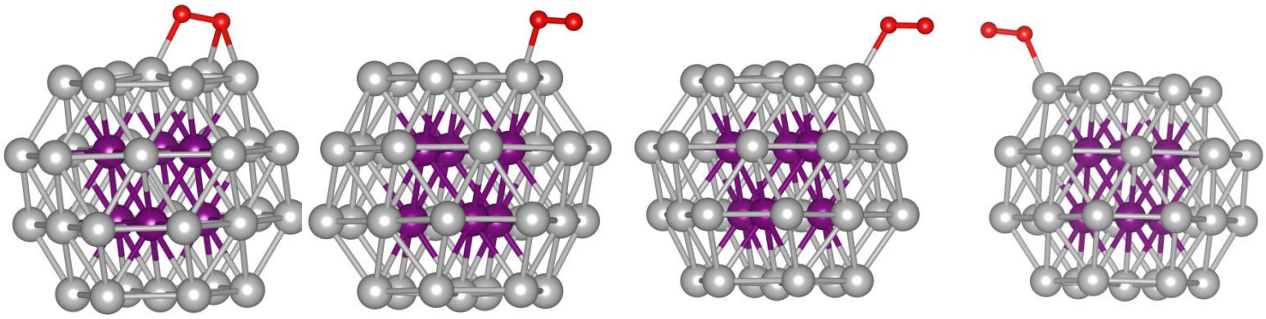

IIA IIB IIC IID

Figure 5. IA,IB,IC,ID represents non optimised structures and IIA,IIB,IIC,IID represents optimised structures of $Ag_{32}Pt_6O_2$.

C. Adsorption of O_2 as a Bridge on $Ag_{32}Pt_6$ nanoalloy at 2 different sites.

Non-Optimized Structure

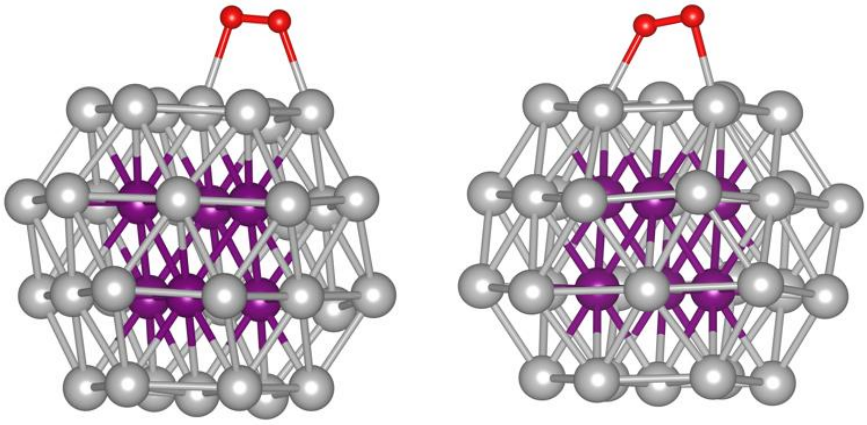

IA IB

Optimized Structure

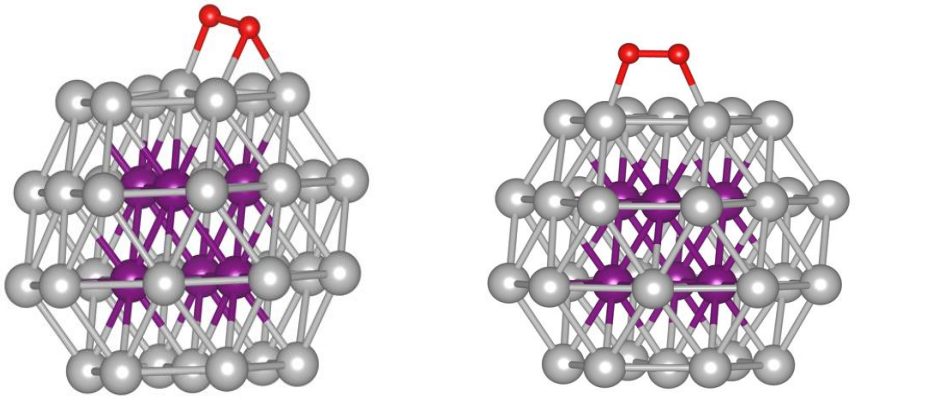

IIA

IIB

Figure 6. IA,IB represents non optimised structures and IIA,IIB represents optimised structures of $Ag_{32}Pt_6O_2$ as bridge.

D. Adsorption of CO on Ag_{38} nanoalloy at 2 different sites.

Non-Optimized Structure

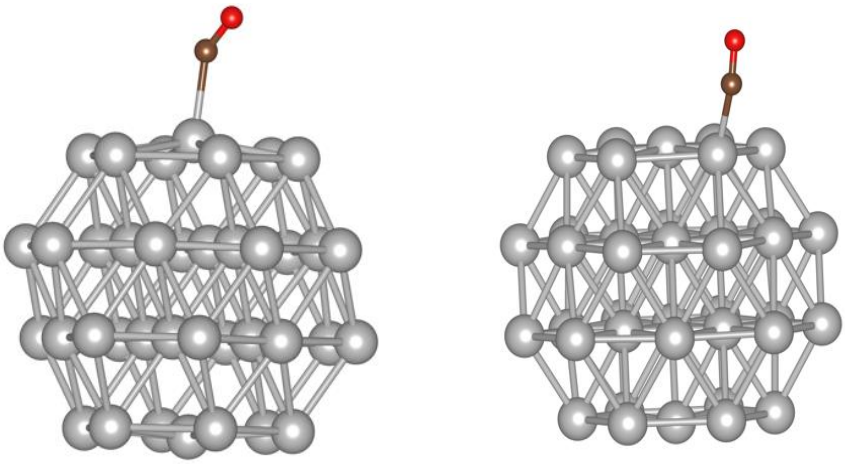

IA IB

Optimized Structure

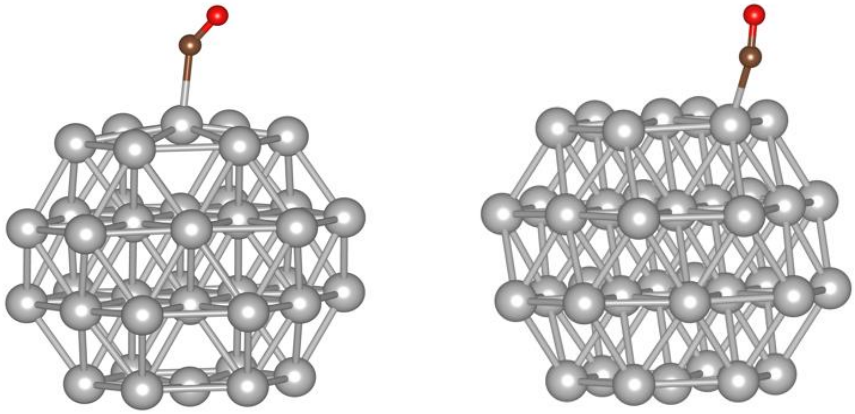

IIA

IIB

Figure 7. IA,IB represents non optimised structures and IIA,IIB represents optimised structures of $Ag_{38}CO$.

E. Adsorption of O_2 on Ag_{38} nanoalloy at 2 different sites.

Non-Optimized Structure

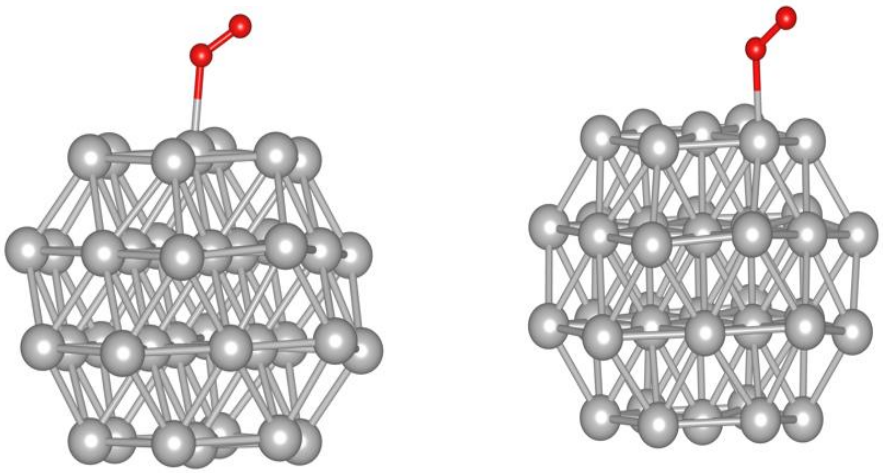

IA IB

Optimized Structure

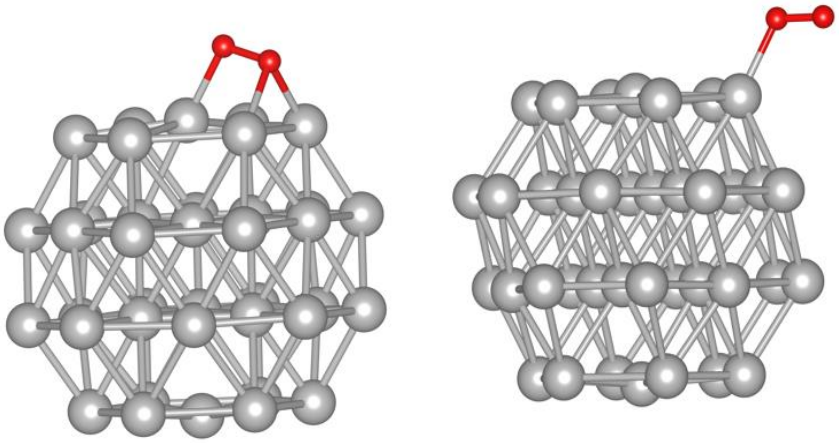

IIA IIB

Figure 8. IA,IB represents non optimised structures and IIA,IIB represents optimised structures of $Ag_{38}O_2$.

F. Adsorption of O_2 as a Bridge on Ag_{38} cluster at 2 different sites.

Non-Optimized Structure

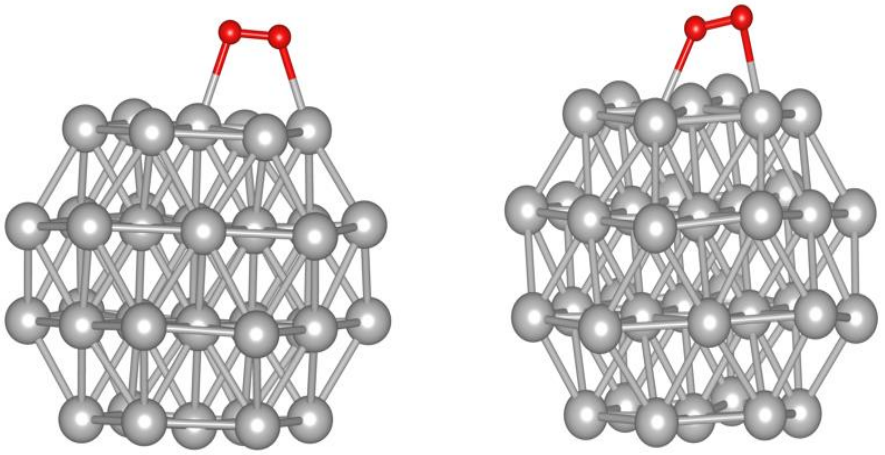

IA IB

Optimized Structure

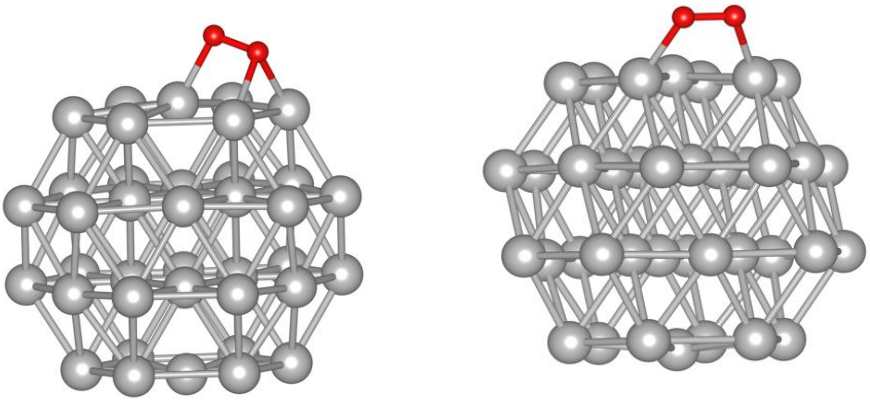

IIA IIB

Figure 9. IA,IB represents non optimised structures and IIA,IIB represents optimised structures of $Ag_{38}O_2$ on Bridge.

G. Bare Structures of $Ag_{32}Pt_6$, Ag_{38}, CO and O_2.

Non-Optimized Structures | Optimized Structures

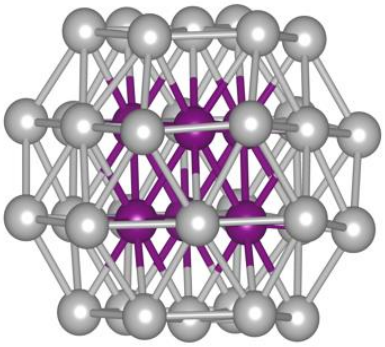

IA

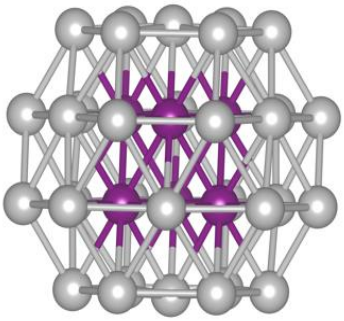

IB

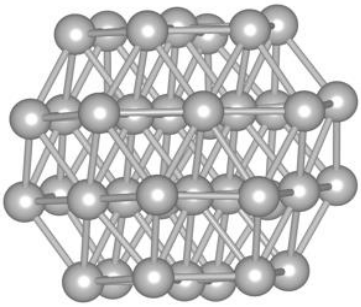

IIA

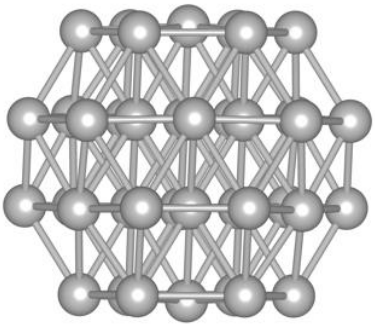

IIB

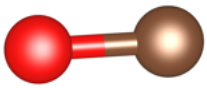

IIIA

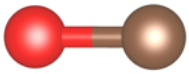

IIIB

IVA

IVB

Figure 10. IA,IIB,IIIC,IVD represents non optimised structures and IA,IIB,IIIC,IVD represents optimised structures..

3.2 Methodology of Bader Charge Analysis

Bader uses zero flux surfaces to divide atoms. A zero flux surface is a 2-D surface on which the charge density is a minimum perpendicular to the surface. Typically in molecular systems, the charge density reaches a minimum between the atoms and this is a natural place to separate atoms from each other. Bader's definition is also useful for charge analysis. The charge enclosed within the bader volume is a good approximation to the total electronic charge of an atom.

Step 1: Geometry optimization- We obtained CO and O_2-adsorbed optimized structures in CONTCAR file from above method described.

Step 2 : Single Point Energy Calculation

- Changing CONTCAR to POSCAR
- In INCAR file, we have to make two key statements TRUE

For reconstructing all the electron densities

LCHARG=.TRUE.
LAECHG = .TRUE.

- NSW=0 for single point energy
- Precision = Accurate

AECCAR0 , AECCAR1 and AECCAR2 files are generated
AECCAR0 = core density
AECCAR1 = Proto atomic valence density
AECCAR2 – SC valence Density

Step 3: Summation of core and valence charge densities

CHGCAR_sum = AECCAR0 + AECCAR2

(CHGCAR_sum contains Electron charge density)

Command: perl chgsum.pl AECCAR0 AECCAR2

Step 4: Using Bader program, Calculating total charge

- Installing Bader Program
- chmod +x bader
- ./bader CHGCAR -ref CHGCAR_sum

ACF.dat file generated which contains bader charge population on each atom of the nanoalloy cluster.

Step 5: Calculating Bader net atomic charge

-Bader net atomic charge = ZVAL - Bader population

ZVAL for Ag = 11.0
ZVAL for Pt = 10.0
ZVAL for C = 4.0
ZVAL for O = 6.0

Charge Analysis- Geometry of $Ag_{32}Pt_6$

There are 8 Ag atoms which have high charge around 0.8 and that Ag atoms are the center of 8 hexagonal faces.

Each hexagonal faces are joined with three hexagonal faces which forms square between them.

Pt inside the core shell are forming octahedral

From this Analysis, We can found 2 adsorption sites to adsorb CO and O_2 on AgPt nanoalloys

Table 1. BADER CHARGE ANALYSIS OF $Ag_{32}Pt_6$

Element		ZVAL	Bader population	Bader Charge
Pt	1	11	10.1971	-0.1971
Pt	2	11	10.1926	-0.1926
Pt	3	11	10.1897	-0.1897
Pt	4	11	10.1963	-0.1963
Pt	5	11	10.1967	-0.1967
Pt	6	11	10.1835	-0.1835
Ag	1	11	10.9829	0.0171
Ag	2	11	10.9758	0.0242
Ag	3	11	10.9815	0.0185
Ag	4	11	10.9845	0.0155
Ag	5	11	10.9746	**0.0254**
Ag	6	11	10.9784	0.0216
Ag	7	11	10.9827	0.0173
Ag	8	11	10.9774	0.0226

Ag	9	11	10.9227	**0.0773**
Ag	10	11	10.9203	**0.0797**
Ag	11	11	10.9180	**0.0820**
Ag	12	11	10.9185	**0.0815**
Ag	13	11	10.9776	0.0224
Ag	14	11	10.9688	**0.0312**
Ag	15	11	10.9736	0.0264
Ag	16	11	10.9842	0.0158
Ag	17	11	10.9187	**0.0813**
Ag	18	11	10.9292	**0.0708**
Ag	19	11	10.9257	**0.0743**
Ag	20	11	10.9183	**0.0817**
Ag	21	11	10.9690	**0.0310**
Ag	22	11	10.9845	0.0155
Ag	23	11	10.9732	0.0268
Ag	24	11	10.9768	0.0232
Ag	25	11	10.9839	0.0161
Ag	26	11	10.9701	**0.0299**
Ag	27	11	10.9748	0.0252
Ag	28	11	10.9850	0.0150
Ag	29	11	10.9731	0.0269
Ag	30	11	10.9864	0.0136
Ag	31	11	10.9832	0.0168
Ag	32	11	10.9705	**0.0295**

Figure 11.

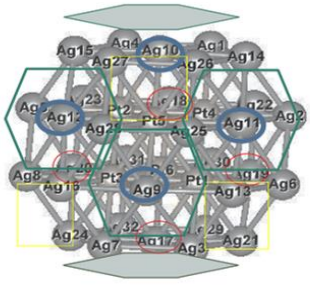

Figure 12.

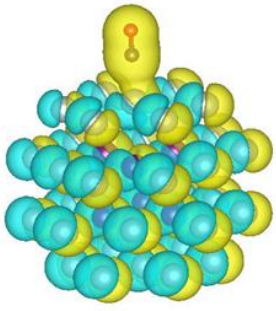

Figure 11. Geometry observation on the basis of charge distribution Figure 12. °Charges on Ag, Pt and CO

Chapter 4

Results and discussion

In the following tables we are taking a specific bond length between C and O of CO, O and O of O_2 from Ag. And taking linear CO and O_2 bond angle of range from 120° to 140°. Then after Optimization, calculating the deviation in them. Also calculating the adsorption energy from the energies of bare clusters.

Table 2. Adsorption of CO molecule on $Ag_{32}Pt_6$

Position		I		II		III		IV	
		Cluster	Optimized	Cluster	Optimized	Cluster	Optimized	Cluster	Optimized
Bond Length (Å)	C-O	1.1400	1.15367	1.1400	1.1517	1.1400	1.1519	1.1400	1.5161
	Ag-C	2.4131	2.1157	2.4171	2.0659	2.4113	2.0672	2.4128	2.0639
Bond Angle		178.1140°	175.184°	178.830°	168.045°	178.502°	166.231°	178.552°	168.807°
Energy (eV)		-116.9974		-117.3477		-117.3472		-117.3492	
Adsorption Energy (eV)		-0.2173		-0.5676		-0.56710		-0.5690	

As we can see here that the adsorption on first position is less that all the other three positions. And the three positions have nearly equal adsorption. This shows the presence of two kinds of geometries.

Table 3. Adsorption of O_2 molecule on $Ag_{32}Pt_6$

Position		I		II		III		IV	
		Cluster	Optimized	Cluster	Optimized	Cluster	Optimized	Cluster	Optimized
Bond Length (Å)	O-O	1.23000	1.39964	1.23000	1.30266	1.23000	1.30295	1.2300	1.3028
	Ag20-O2	2.41032	2.2355	2.40301	2.17806	2.40731	2.17564	2.4011	2.1736
	Ag5-O1	3.8294	2.3119						
	Ag8-O1	3.6035	2.3004						
Bond Angle		130.054°	107.9021°	132.653°	115.067°	125.126°	114.311°	135.870°	113.439°
Energy (eV)		-112.18549		-111.90138		-111.90073		-111.9030	
Adsorption Energy (eV)		-0.34339		-0.05928		-0.05862		-0.06090	

As we can see here that the adsorption on first is more than other three positions. And adsorption on other three positions are nearly equal.

Table 4. Adsorption of O_2 molecule as bridge on $Ag_{32}Pt_6$

Position		**I**		**II**		
		Cluster	**Optimized**	**Cluster**		**Optimized**
Bond Length (Å)	**O-O**	1.2300	1.3989	1.2300		1.3463
	Ag20-O2	2.4048	2.2363	**Ag24-O2**	2.4011	2.2326
	Ag8-O1	2.4025	2.3051	**Ag8-O1**	2.4099	2.2327
	Ag5-O1	3.7596	2.3084			
Energy (eV)		-112.1857		-112.1713		
Adsorption Energy (eV)		**-0.3459**		**-0.3315**		

In the case of bridge, the adsorption is nearly equal in both the cases.

Table 5. Adsorption of CO molecule on Ag_{38}					
Position		**I**		**II**	
		Cluster	**Optimized**	**Cluster**	**Optimized**
Bond Length (Å)	**C-O**	1.1400	1.1518	1.1400	1.15177
	Ag-C	2.4131	2.3155	2.4171	2.12332
Bond Angle		178.1140	144.8443	178.830	156.9817
Energy (eV)		**-96.7235**		**-97.08490**	
Adsorption Energy (eV)		**-0.0150**		**-0.3765**	

As we compare the adsorption energy of Ag_{38} cluster with $Ag_{32}Pt_6$ nanoalloy, we get to know that adsorption energy for CO in case of Ag_{38} is less for both the sites.

Table 6. Adsorption of O_2 molecule on Ag_{38}						
Position		**I**		**II**		
		Cluster	**Optimized**	**Cluster**		**Optimized**
Bond Length (Å)	**O1-O2**	1.2300	1.4145	1.2300		1.3028
	Ag26-O2	2.41032	2.2066	**Ag14-O2**	2.40112	2.1848
	Ag14-O1	3.8294	2.2806			
	Ag11-O1	3.6035	2.2750			
Bond Angle O1-O2-Ag26		130.054°	106.4052°	132.068°		117.7766°
Energy (eV)		-92.2035		-91.8166		
Adsorption Energy		**-0.4354**		**-0.0484**		

The adsorption of O_2 is more in case of Ag_{38} as that of $Ag_{32}Pt_6$ for all the possible sites.

Table 7. Adsorption of O_2 molecule as bridge on $Ag_{32}Pt_6$						
Position		**I**		**II**		
		Cluster	**Optimized**	**Cluster**		**Optimized**
Bond Length (Å)	**O-O**	1.2300	1.4144	1.2300		1.3570
	Ag26-O2	2.4048	2.2123	**Ag30-O2**	2.40112	2.1859
	Ag14-O1	2.4025	2.2746	**Ag14-O1**	2.4099	2.1835
	Ag30-O1	3.2262	2.2753			
Energy (eV)		-92.3159 eV		-92.2297 eV		
Adsorption Energy (eV)		**-0.5477 eV**		**-0.4615eV**		

The adsorption of O_2 as a bridge is also more in case of Ag_{38} as that of $Ag_{32}Pt_6$ for all the possible sites.

Table 8. Optimization of Bare Structures of $Ag_{32}Pt_6$, Ag_{38}, CO and O_2.		
Energy (eV)	$Ag_{32}Pt_6$	-101.9798
	Ag_{38}	-81.908
	CO	-14.8003
	O_2	-9.8623

After Calculating adsorption energy we are now trying to verify our results with the help of Bader charge, trying to figure out why at some specific position adsorption is more while on other it has less adsorption.
In our mythology section we have already mentioned how we calculated Bader charge.

Table 9. BADER CHARGE ANALYSIS OF $Ag_{32}Pt_6$				
Element		ZVAL	Bader population	Bader Charge
Pt	2	10	10.1926	-0.1926
Pt	3	10	10.1897	-0.1897
Pt	5	10	10.2	-0.1967
Pt	6	10	10.1835	-0.1835
Ag	5	11	10.98	0.0168
Ag	8	11	10.97	0.0295
Ag	20	11	10.9183	0.0817

Table 10. BADER CHARGE ANALYSIS OF $Ag_{32}Pt_6CO$				
Element		ZVAL	Bader population	Bader Charge
Pt	2	10	10.2127	-0.2127
Pt	3	10	10.2176	-0.2176
Pt	5	10	10.1954	-0.1954
Pt	6	10	10.2094	-0.2094
Ag	5	11	10.9810	0.0190
Ag	8	11	10.9806	0.0194
Ag	20	11	10.7737	0.2263
C	1	4	2.8419	1.1581
O	1	6	7.2271	-1.2271

Adsorption Energy: **-0.2173 eV**

Table 11. BADER CHARGE ANALYSIS OF $Ag_{32}Pt_6CO$				
Element		ZVAL	Bader population	Bader Charge
Pt	2	10	10.1802	-0.1802
Pt	3	10	10.2253	-0.2253
Pt	5	10	10.1888	-0.1888
Pt	6	10	10.1968	-0.1968
Ag	5	11	10.9752	0.0248
Ag	8	11	10.8482	0.1518
Ag	20	11	10.9263	0.0737
C	1	4	2.8084	1.1916
O	1	6	7.2333	-1.2333

Adsorption Energy: **-0.5676 eV**

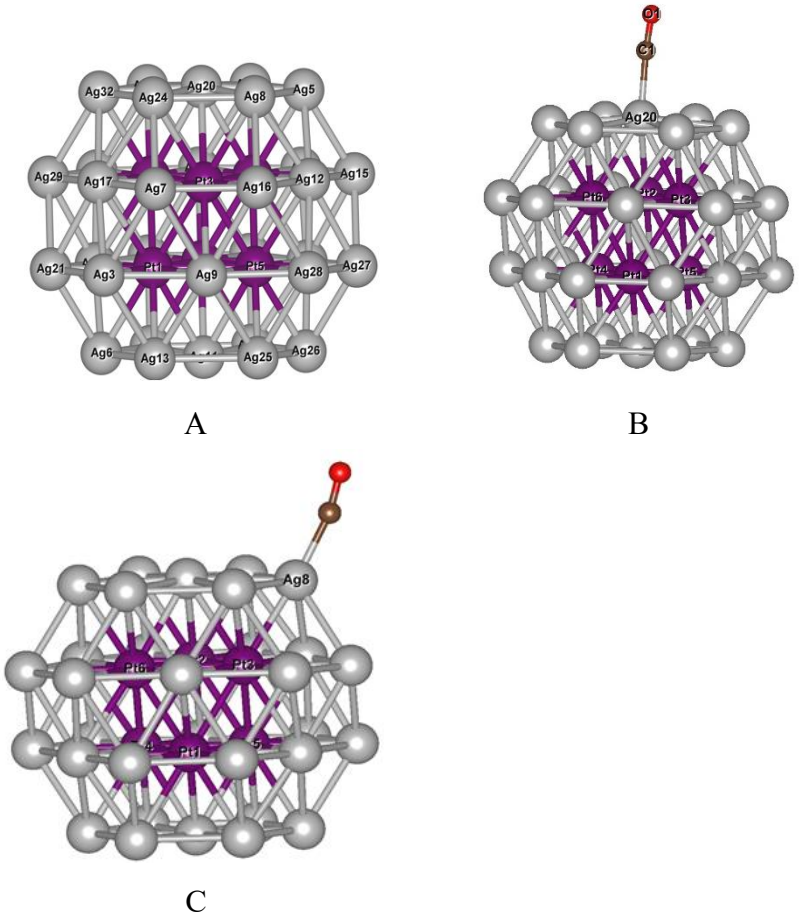

A B C

Figure 13. A,B,C represents numbering on $Ag_{32}Pt_6$ nanoalloy.

Table 12. BADER CHARGE ANALYSIS OF Ag_{38}				
Element		ZVAL	Bader population	Bader Charge
Ag	14	11	11.0036	-0.0036
Ag	26	11	10.9951	0.0049

Table 13. BADER CHARGE ANALYSIS OF CO				
Element		ZVAL	Bader population	Bader Charge
C	1	4	2.7596	1.2404
O	1	6	7.2404	-1.2404

Table 14. BADER CHARGE ANALYSIS OF $Ag_{38}CO$				
Element		ZVAL	Bader population	Bader Charge
Ag	26	11	10.8887	0.1113
C	1	4	2.82	1.1810
O	1	6	7.23	-1.2276

Adsorption energy: **-0.0150 eV**

Table 15. BADER CHARGE ANALYSIS OF $Ag_{38}CO$				
Element		ZVAL	Bader population	Bader Charge
Ag	14	11	10.8821	0.1179
C	1	4	2.78	1.2176
O	1	6	7.25	-1.2503

Adsorption energy: **-0.3765 eV**

As we compare the adsorption energy data of $Ag_{32}Pt_6CO$ (Table 10 and 11) the difference is due to back bonding and in the case of $Ag_{38}CO$ (Table 14 and 15) the difference is due to charge transfer, the reason for more adsorption energy of $Ag_{32}Pt_6CO$ as compare to $Ag_{38}CO$ might be the donation of extra electron density from Pt to CO.

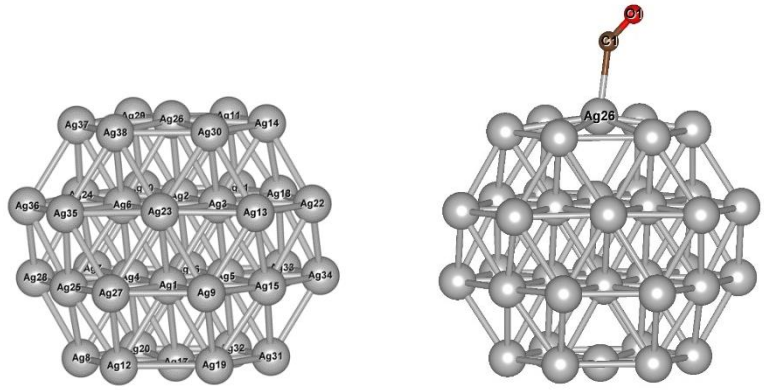

A

B

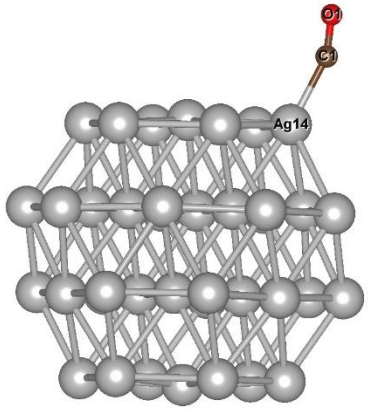

C

Figure 14. A, B, C represents numbering on Ag_{38} nanocluster.

Table 16. BADER CHARGE ANALYSIS OF $Ag_{32}Pt_6$				
Element		**ZVAL**	**Bader population**	**Bader Charge**
Pt	2	10	10.1926	-0.1926
Pt	3	10	10.1897	-0.1897
Pt	5	10	10.2	-0.1967
Pt	6	10	10.1835	-0.1835
Ag	5	11	10.98	0.0168
Ag	8	11	10.97	0.0295
Ag	20	11	10.9183	0.0817

Table 17. BADER CHARGE ANALYSIS OF $Ag_{32}Pt_6O_2$				
Element		**ZVAL**	**Bader population**	**Bader Charge**
Pt	2	10	10.1960	-0.1960
Pt	3	10	10.2087	-0.2086
Pt	5	10	10.1893	-0.1892
Pt	6	10	10.1970	-0.1970
Ag	5	11	10.8074	0.1925
Ag	8	11	10.8125	0.1874
Ag	20	11	10.754	0.2451

Adsorption energy: **-0.34339 eV**

Table 18. BADER CHARGE ANALYSIS OF $Ag_{32}Pt_6O_2$				
Element		**ZVAL**	**Bader population**	**Bader Charge**
Pt	2	10	10.1846	-0.1845
Pt	3	10	10.2150	-0.2150
Pt	5	10	10.1846	-0.1845
Pt	6	10	10.1794	-0.1793
Ag	5	11	10.9402	0.059
Ag	8	11	10.8180	0.1820
Ag	20	11	10.8806	0.11937

Adsorption energy: **-0.05928 eV**

As we can see from the above Table (i.e. Table 17 and 18) that adsorption is more in first case as compare to second case because there is formation of the bridge in first case. Due to bridge more surface area is covered, means more adsorption.

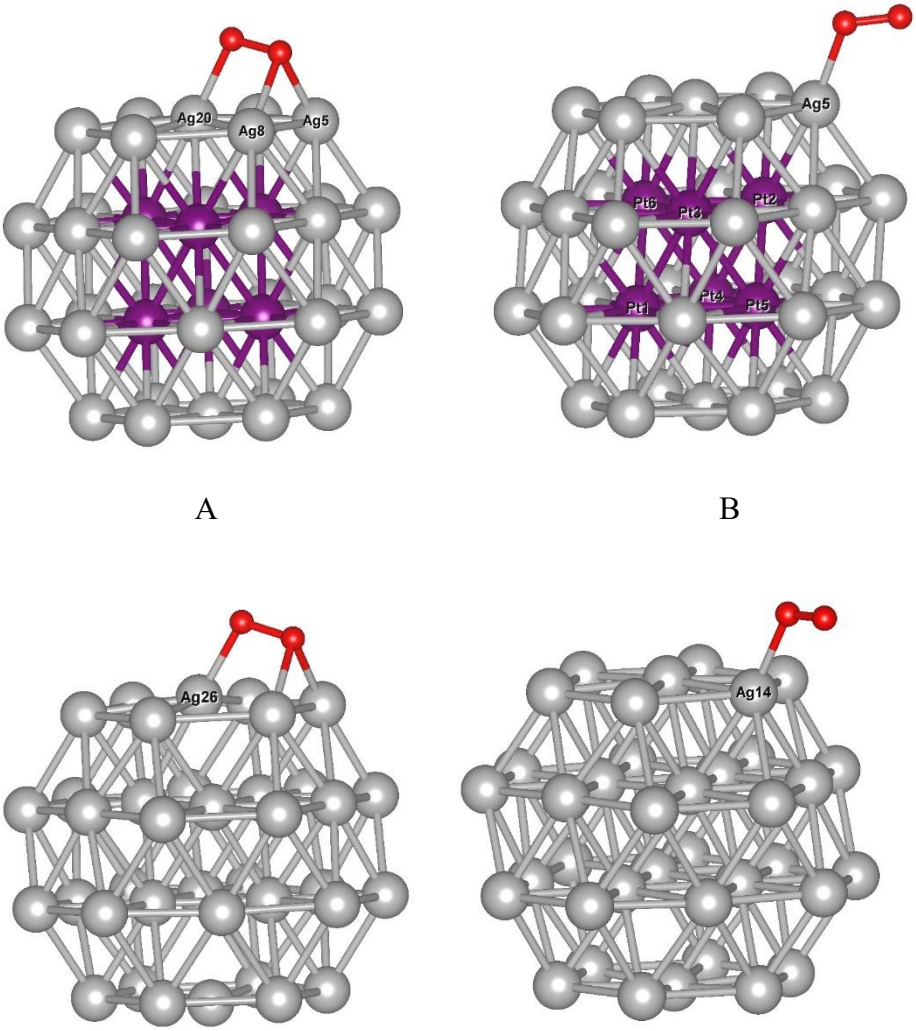

A B

C D

Figure 15. A, B represents numbering on $Ag_{32}Pt_6$ nanoalloy. C, D represents numbering on Ag_{38} nanocluster.

Table 19. BADER CHARGE ANALYSIS OF Ag_{38}				
Element		**ZVAL**	**Bader population**	**Bader Charge**
Ag	14	11	11.0036	-0.0036
Ag	26	11	10.9951	0.0049

Table 20. BADER CHARGE ANALYSIS OF $Ag_{38}O_2$				
Element		**ZVAL**	**Bader population**	**Bader Charge**
Ag	26	11	10.981047	0.018953

Adsorption energy: -0.4354 eV

Table 21. BADER CHARGE ANALYSIS OF $Ag_{38}O_2$				
Element		**ZVAL**	**Bader population**	**Bader Charge**
Ag	14	11	10.8388	0.1612

Adsorption energy: -0.0484 eV

As we can see from the above Table (i.e. Table 20 and 21) that adsorption in first case is more and the reason behind this is bridge formation. Bridge formation increases the covered surface area mean increase in adsorption.

As we can see from our above data (i.e. Table 17 and 20), the magnitude of positive charge on Ag, in case of bare Ag 38 cluster is, less than that of $Ag_{32}Pt_6$ nanoalloy, because Pt is more electronegative element and it will take electron density from Ag and make it electron deficient. So in case of bare Ag_{38} cluster back donation of electron density will be more as compare to $Ag_{32}Pt_6$,(back donation of electron density means Ag will give its electron density to the vacant antibonding orbital of O_2) so more charge transfer will happen in the case of Ag_{38} means more strong bond will form. Therefore adsorption energy is high in case of Ag_{38}.

Feasible conditions for CO oxidation-

1. Not much strong adsorption of O_2 on the surface, that the removal of directly adsorbed O will become difficult.

2. Adsorption strength of CO should be less than O_2, so that CO poisoning would not happen.

Mechanism of CO oxidation-

As O_2 is adsorbed on the surface of cluster, the bond length of adsorbed O will increase, means its stretching frequency will decrease so now this bond between two O-atom can easily be broken. After bond breaking, the atomic O will react with adsorbed CO and result into the formation of CO_2, which will be desorbed from the surface. Same mechanism will be followed by the other oxygen atom, which is directly adsorbed to the surface, and in this way, CO oxidation happen.

In our project, conditions of CO oxidation are more feasible on $Ag_{32}Pt_6$ than that of Ag_{38}. Because in case of $Ag_{32}Pt_6$, Pt will attract the electron density from Ag and make it electron deficient so adsorption of O_2 will not be much strong so that the O which is directly adsorbed to the surface can participate in CO oxidation. Also the adsorption of CO is less than that of O_2 so CO poisoning will not happen. [34]

Table 22. Adsorption of O_2 molecule on $Ag_{32}Pt_6$

Position		**I**	
		Cluster	**Optimized**
Bond Length (Å)	**O-O**	1.2300	1.3466
	Ag24-O2	2.40112	2.2317
	Ag8-O1	3.7597	2.2305
Bond Angle		132.068°	109.317°
Energy eV		-112.1708	
Adsorption Energy eV		**-0.3287**	

Chapter 5

Conclusion

As we have seen in results, our developed cluster $Ag_{32}Pt_6$ is working efficiently. It provides very suitable conditions to O_2 for the reaction of our interest. Unlike Ag_{38}, in our cluster-$Ag_{32}Pt_6$, the electron density of Ag is also shared by Pt, which makes Ag electron deficient. The desorption of directly attached O_2 becomes easier for this electron deficient Ag. Another advantage is that the adsorption of CO is also comparatively lesser, which will check the possibilities of CO poisoning.

5.1 Future Work

As we have considered all the possibilities of CO and O_2 adsorption on $Ag_{32}Pt_6$ and also checked that CO oxidation is possible on our cluster-$Ag_{32}Pt_6$. Now the next step is doing reaction on our cluster-$Ag_{32}Pt_6$.

Reference

(1) Ferrando, R.; Jellinek, J.; Johnston, R. L. Nanoalloys: From Theory to Applications of Alloy Clusters and Nanoparticles. *Chem Rev* **2008**, *108*, 845–910 (3)

(2) Zafeiratos, S.; Piccinin, S.; Teschner, D. Alloys in Catalysis: Phase Separation and Surface Segregation Phenomena in Response to the Reactive Environment. *Catal Sci Technol* **2012**, *2*, 1787 (9)

(3) Stamenkovic, V. R.; Mun, B. S.; Arenz, M.; Mayrhofer, K. J. J.; Lucas, C. A.; Wang, G.; Ross, P. N.; Markovic, N. M. Trends in Electrocatalysis on Extended and Nanoscale Pt-Bimetallic Alloy Surfaces. *Nat Mater* **2007**, *6*, 241–247 (3)

(4) Aldirmaz, E.; Guler, M.; Guler, E.; Dere, A.; Tataroğlu, A.; Al-Sehemi, A. G.; Al-Ghamdi, A. A.; Yakuphanoglu, F. A Shape Memory Alloy Based on Photodiode for Optoelectronic Applications. *J Alloys Compd* **2018**, *743*, 227–233 (19)

(5) Gao, J.; Ren, X.; Chen, D.; Tang, F.; Ren, J. Bimetallic Ag–Pt Hollow Nanoparticles: Synthesis and Tunable Surface Plasmon Resonance. *Scr Mater* **2007**, *57*, 687–690 (8)

(6) Yu, W.; Porosoff, M. D.; Chen, J. G. Review of Pt-Based Bimetallic Catalysis: From Model Surfaces to Supported Catalysts. *Chem Rev* **2012**, *112*, 5780–5817 (11)

(7) Olobardi, S.; Vega, L.; Fortunelli, A.; Stener, M.; Viñes, F.; Neyman, K. M. Optical Properties and Chemical Ordering of Ag–Pt Nanoalloys: A Computational Study. *The Journal of Physical Chemistry C* **2019**, *123*, 25482–25491 (41)

(8) Danielis, N.; Vega, L.; Fronzoni, G.; Stener, M.; Bruix, A.; Neyman, K. M. AgPd, AuPd, and AuPt Nanoalloys with Ag- or Au-Rich

Compositions: Modeling Chemical Ordering and Optical Properties. *The Journal of Physical Chemistry C* **2021**, *125* (31), 17372–17384

(9) Zhao, Z.; Fisher, A.; Shen, Y.; Cheng, D. Magnetic Properties of Pt-Based Nanoalloys: A Critical Review. *J Clust Sci* **2016**, *27*, 817–843(3)

(10) Mondal, K.; Banerjee, A.; Ghanty, T. K. Structural and Chemical Properties of Subnanometer-Sized Bimetallic Au_{19} Pt Cluster. *The Journal of Physical Chemistry C* **2014**, *118* (22), 11935–11945 (12)

(11) Piotrowski, M. J.; Piquini, P.; Da Silva, J. L. F. Platinum-Based Nanoalloys $Pt_n TM_{55-n}$ (TM = Co, Rh, Au): A Density Functional Theory Investigation. *The Journal of Physical Chemistry C* **2012**, *116* (34), 18432–18439 (9)

(12) Semiz, L.; Abdullayeva, N.; Sankir, M. Nanoporous Pt and Ru Catalysts by Chemical Dealloying of Pt-Al and Ru-Al Alloys for Ultrafast Hydrogen Generation. *J Alloys Compd* **2018**, *744*, 110–115

(13) Negreiros, F. R.; Taherkhani, F.; Parsafar, G.; Caro, A.; Fortunelli, A. Kinetics of Chemical Ordering in a Ag-Pt Nanoalloy Particle via First-Principles Simulations. *J Chem Phys* **2012**, *137* 194302 (19)

(14) Paz-Borbón, L. O.; Johnston, R. L.; Barcaro, G.; Fortunelli, A. Structural Motifs, Mixing, and Segregation Effects in 38-Atom Binary Clusters. *J Chem Phys* **2008**, *128*, 134517 (13)

(15) Rapetti, D.; Ferrando, R. Density Functional Theory Global Optimization of Chemical Ordering in AgAu Nanoalloys. *J Alloys Compd* **2019**, *779*, 582–589 (2)

(16) Serpell, C. J.; Cookson, J.; Ozkaya, D.; Beer, P. D. Core@shell Bimetallic Nanoparticle Synthesis via Anion Coordination. *Nat Chem* **2011**, *3* (6), 478–483 (12)

(17) Yun, K.; Cho, Y.-H.; Cha, P.-R.; Lee, J.; Nam, H.-S.; Oh, J. S.; Choi, J.-H.; Lee, S.-C. Monte Carlo Simulations of the Structure of Pt-Based Bimetallic Nanoparticles. *Acta Mater* **2012**, *60* (12), 4908–4916 (9)

(18) Deng, L.; Deng, H.; Xiao, S.; Tang, J.; Hu, W. Morphology, Dimension, and Composition Dependence of Thermodynamically Preferred Atomic Arrangements in Ag–Pt Nanoalloys. *Faraday Discuss* **2013**, *162*, 293 (16)

(19) Rodríguez-Kessler, P. L.; Muñoz-Castro, A.; Alonso-Dávila, P. A.; Aguilera-Granja, F.; Rodríguez-Domínguez, A. R. Structural, Electronic and Catalytic Properties of Bimetallic Pt Ag (N=1–7) Clusters. *J Alloys Compd* **2020**, *845*, 155897 (4)

(20) Wisniewska, J.; Guesmi, H.; Ziolek, M.; Tielens, F. Stability of Nanostructured Silver-Platinum Alloys. *J Alloys Compd* **2019**, *770*, 934–941 (15)

(21) Mendes, P. C. D.; Justo, S. G.; Mucelini, J.; Soares, M. D.; Batista, K. E. A.; Quiles, M. G.; Piotrowski, M. J.; Da Silva, J. L. F. *Ab Initio* Insights into the Formation Mechanisms of 55-Atom Pt-Based Core–Shell Nanoalloys. *The Journal of Physical Chemistry C* **2020**, *124* (1), 1158–1164 (12)

(22) Mendes, P. C. D.; Justo, S. G.; Mucelini, J.; Soares, M. D.; Batista, K. E. A.; Quiles, M. G.; Piotrowski, M. J.; Da Silva, J. L. F. Ab Initio Insights into the Formation Mechanisms of 55-Atom Pt-Based Core–Shell Nanoalloys. J. Phys. Chem. C 2020, 124 (1), 1158–1164 (6)

(23) Ojha, A.; Megha; Bulusu, S. S.; Banerjee, A. Structure and Dynamics of 38-Atom Ag-Pt Nanoalloys Using ANN Based-Interatomic Potential. *Comput. Theor. Chem.* **2023**, *1220*, 113985 (7)

(24) Wisniewska, J.; Guesmi, H.; Ziolek, M.; Tielens, F. Stability of Nanostructured Silver-Platinum Alloys. J. Alloys Compd. 2019, 770, 934–941 (34)

(25) Ferrari, P.; Molina, L. M.; Kaydashev, V. E.; Alonso, J. A.; Lievens, P.; Janssens, E. Controlling the Adsorption of Carbon Monoxide on Platinum Clusters by Dopant-Induced Electronic Structure Modification. *Angewandte Chemie* **2016**, *128* (37), 11225–11229 (9)

(26) Shao, T.; Bai, D.; Qiu, M.; Li, Y.; Zhang, Q.; Xue, Z.; He, S.; Zhang, D.; Zhou, X. Facile Synthesis of AgPt Nano-Pompons for Efficient Methanol Oxidation: Morphology Control and DFT Study on Stability Enhancement. *Journal of Industrial and Engineering Chemistry* **2022**, *108*, 456–465 (5)

(27) Jeyaprabha, C.; Sathiyanarayanan, S.; Venkatachari, G. Co-Adsorption Effect of Polyaniline and Halide Ions on the Corrosion of Iron in 0.5M H2SO4 Solutions. *Journal of Electroanalytical Chemistry* **2005**, *583* (2)

(28) He, W.; Wu, X.; Liu, J.; Zhang, K.; Chu, W.; Feng, L.; Hu, X.; Zhou, W.; Xie, S. Formation of AgPt Alloy Nanoislands via Chemical Etching with Tunable Optical and Catalytic Properties. *Langmuir* **2010**, *26* (6)

(28) He, W.; Wu, X.; Liu, J.; Zhang, K.; Chu, W.; Feng, L.; Hu, X.; Zhou, W.; Xie, S. Pt-Guided Formation of Pt−Ag Alloy Nanoislands on Au Nanorods and Improved Methanol Electro-Oxidation. *The Journal of Physical Chemistry C* **2009**, *113* (24)

(29) Negreiros, F. R.; Halder, A.; Yin, C.; Singh, A.; Barcaro, G.; Sementa, L.; Tyo, E. C.; Pellin, M. J.; Bartling, S.; Meiwes-Broer, K.; Seifert, S.; Sen, P.; Nigam, S.; Majumder, C.; Fukui, N.; Yasumatsu, H.; Vajda, S.; Fortunelli, A. Bimetallic Ag-Pt Sub-

nanometer Supported Clusters as Highly Efficient and Robust Oxidation Catalysts. *Angewandte Chemie International Edition* **2018**, *57* (5)

(30) Hwang, S. Y.; Zhang, C.; Yurchekfrodl, E.; Peng, Z. Property of Pt–Ag Alloy Nanoparticle Catalysts in Carbon Monoxide Oxidation. *The Journal of Physical Chemistry C* **2014**, *118* (49)

(31) Hafner, J. Ab-Initio Simulations of Materials Using VASP:Density-Functional Theory and Beyond. J. Comput. Chem.

(32) Massoud, R. A.; Makhyoun, M. A. Theoretical Study of the Interaction of Ethanol with the (3,5-Dimethylpyrazole-N2)(N-Salicylidenephenyl-Alaninato-O,N,O′)Copper(II) Complex. *J Struct. Chem.* **2019**, *60* (6)

(33) Heydon, A.; Levin, R.; Mann, T.; Yu, Y. The Vesta Approach to Software Configuration Management

(34) Chen, Z. W.; Wen, Z.; Jiang, Q. Rational Design of Ag_{38} Cluster Supported by Graphdiyne for Catalytic CO Oxidation. *J. Phys. Chem. C* **2017**, *121* (6)